

XCAT-2.0: A Comprehensive Library of Personalized Digital Twins Derived from CT Scans

Lavsen Dahal^{a,b}, Mobina Ghoghnejad^a, Dhruvajyoti Ghosh^{a,c}, Yubraj Bhandari^a,
David Kim^{a,b}, Fong Chi Ho^{a,b}, Fakrul Islam Tushar^{a,b}, Ehsan Abadi^{a,b}, Ehsan Samei^{a,b},
Joseph Lo^{a,b+}, Paul Segars^{a+}

^aCenter for Virtual Imaging Trials, Carl E. Ravin Advanced Imaging Laboratories, Department of Radiology, Duke University School of Medicine, Durham, NC, 27708, USA

^bElectrical and Computer Engineering, Pratt School of Engineering, Duke University, Durham, NC, 27708, USA

^cDepartment of Biostatistics & Bioinformatics, Duke University School of Medicine, Durham, NC, 27708, USA

+Co-Senior Authors

ARTICLE INFO

Keywords: Computational Phantoms, Segmentation, Human Digital Twin, Computed Tomography, Neural Networks, Virtual Imaging Trials

ABSTRACT

Virtual Imaging Trials (VIT) offer a cost-effective and scalable approach for evaluating medical imaging technologies. Computational phantoms, which mimic real patient anatomy and physiology, play a central role in VIT. However, the current libraries of computational phantoms face limitations, particularly in terms of sample size and diversity. Insufficient representation of the population hampers accurate assessment of imaging technologies across different patient groups. Traditionally, phantoms were created by manual segmentation, which is a laborious and time-consuming task,

impeding the expansion of phantom libraries. This study presents a framework for realistic computational phantom modeling using a suite of four deep learning segmentation models, followed by three forms of automated organ segmentation quality control. Over 2500 computational phantoms with up to 140 structures illustrating a sophisticated approach to detailed anatomical modeling are released. Phantoms are available in both voxelized and surface mesh formats. The framework is aggregated with an in-house CT scanner simulator to produce realistic CT images. The framework can potentially advance virtual imaging trials, facilitating comprehensive and reliable evaluations of medical imaging technologies. Phantoms may be requested at <https://cvit.duke.edu/resources/>, code, model weights, and sample CT images are available at <https://xcat-2.github.io>.

1. Introduction

Virtual Imaging Trials (VIT) offer cost-effectiveness, speed and scalability in the evaluation and optimization of existing medical imaging technologies compared to traditional clinical trials [1-4].

VIT requires a virtual patient population that emulates the anatomy and physiology of the patient using computational anthropomorphic phantoms. These computational phantoms are expected to realistically represent the true population in terms of relevant trial characteristics such as body habitus, organ volumes, tissue properties, and blood flow.

A considerable development of computational phantoms have been evolved from geometric models in the 1960s [5] to advanced NURBS-based XCAT phantoms in recent years [6]. The comprehensive full body phantoms for adult male and female based on the Visible Male and Female datasets [7] were built in early 2000[8]. The computational phantoms of the male and female newborn patients defined using Nonuniform rational B-spline (NURBS) surfaces followed quickly [9]. In the subsequent years, the phantoms library expanded to include 60 adult and 90 pediatric computational phantoms, covering a range of ages, heights, and body mass percentiles [10, 11]. The development of computational phantoms is summarized in [12, 13].

Despite widespread use, the current phantom library sample size is inadequate for use in virtual imaging studies. Several studies have shown that sample size in thousands is required to improve the reliability of the virtual imaging trials [14-16]. However, the generation of computational phantoms has faced significant challenges due to the painstakingly slow process of manual organ segmentation with skilled expertise, which is still prone to human variability. This bottleneck has impeded the expansion of phantom libraries that can realistically represent the population at large.

A recent approach by [17] aimed to automate phantom generation from radiological images but lacked quality due to insufficient segmentation algorithms in terms of quality and number of organs segmented. However, recent advancements in deep learning have improved segmentation[18-22], enabling the creation of patient specific phantoms with accurate organ geometry representation. TotalSegV2[18] has catalogued 117 anatomical structures, while the Segment Anything Model[21] excels in 2D segmentation but performs poorly in 3D medical image segmentation[23]. Despite

rapid advancements in the field, none of these models fully address the issues of segmentation failures or implement comprehensive quality control. Our major contributions are summarized below:

1. **Automated Quality Control:** We uniquely integrate automated quality control in three distinct ways to effectively address segmentation failures.
2. **Dual Output Formats:** We provide both voxel and mesh output formats for over 2500 anatomical models, enriched with critical metadata such as race, sex, age, and body habitus. This dual-format approach with metadata not only enhances 3D applications but also significantly advances the current research in medical imaging segmentation.
3. **High-Resolution Meshes:** In addition to the commonly used voxel format in medical image segmentation, we release high-resolution, geometrically accurate mesh representations. These are crucial for detailed anatomical studies, surgical planning, and virtual reality simulations, allowing for smoother visualizations and more precise model interactions.

2. **Methods**

2.1 *Data Curation*

Four datasets with a total of 3400 CT volumes were utilized to develop the segmentation model, as presented in Table 1 and Table 2. The public dataset associated with TotalSegmentator [18] and a private dataset from Duke University Health System were used for model development and validation, while three other public datasets were used for external testing: CT_ORG [24], ABDOMEN_1K [25], AMOS [26] and XCAT [10, 11]. To create phantoms, the finalized model was applied to a separate dataset of 3581 CT volumes from Duke University Health System. The inclusion criteria for the dataset consisted of CT volumes acquired between January 1, 2014, and

March 30, 2023, utilizing protocols that include PET/CT and chest-abdomen-pelvis scans, ensuring a comprehensive coverage of the whole body.

Our model training drew upon public and private data that were pseudo-labeled with a combination of public and private segmentation models. This approach allows us to expand the training data and incorporate a wider range of anatomical variations and complexities. The training data of 990 patient CT volumes comprised 489 patients selected from the 600 in the TotalSegmentator [18] dataset that contained full-body structures and 501 from the Duke CT dataset which were randomly sampled. For the TotalSegmentator cases, the provided labels were applied. For Duke data, pseudo-labels of organ masks were generated automatically using a combination of three models. The TotalSegmentator model was used to label 104 structures while a proprietary commercial model was used to label 33 structures. Additionally, the MOOSE public body composition model [22], created labels for visceral fat, subcutaneous fat, and muscles.

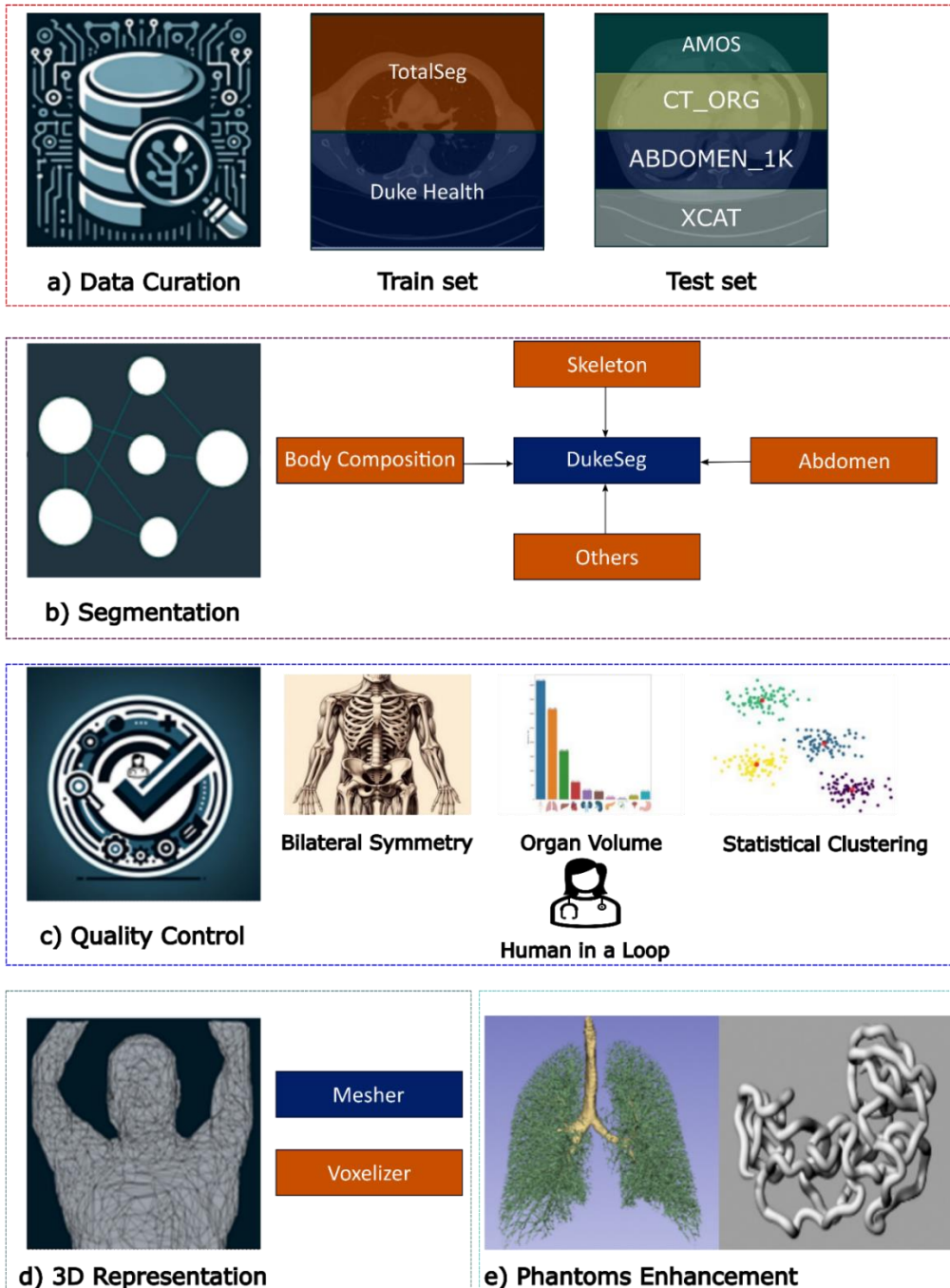


Figure 1 Overview of the Methodology: This figure illustrates the five-module approach used in our study. (a) Data Curation: Collects data from various public and private repositories to train and test the deep learning-based segmentation model, DukeSeg. (b) DukeSeg Model: An in-house developed segmentation tool consisting of four distinct models tailored for segmenting different anatomical structures. (c) Quality Control: Utilizes four types of quality assessments, validated by an MD to ensure accuracy through a human-in-the-loop approach. (d) 3D Representation: Represents the 3D segmentation results in mesh or voxel formats. (e) Detailed Modeling: Includes mathematical modeling of intricate anatomical details such as the small intestine, and airways and vessels.

Table 1 Split for Train and Test utilizing various public and private datasets.

Dataset	#Train	#Test
TotalSegmentator	489	-
DukeCT	501	-
CT_ORG	-	140
ABDOMEN_1K	-	1000
AMOS	-	200
XCAT	-	50
Total	990	1420

Table 2 Characteristics of Training set

Dataset	Totalseg	DukeCT
#Patients	489	501
Male	288	354
Female	201	147
Age (years)	63.5(14.9)	62.1(16.3)
Weight (kg)	-	86.5(23.1)
Height (m)	-	1.73(0.10)
Slice thickness	1.5mm	0.625, 3.75 mm

2.2 Deep Learning Based Segmentation

The nnU-Net deep learning-based method [27] was trained as a set of four models, each specializing in segmenting different sets of structures. The first model segmented the body outline, subcutaneous fat, visceral fat, and muscles. The second model focused exclusively on bone segmentation, encompassing a set of 62 classes. The third model segmented a total of 13 classes focusing on the internal organs in the abdomen region and the esophagus. Meanwhile, the final model segmented 61 structures not covered by the first three models thereby providing covering a diverse range of anatomical structures.

2.3 Quality Control

As with any segmentation approach, failures can occur due to factors like poor image quality or limitations of the model. To address the potential failure, we employed three quality control

approaches: bilateral symmetry, volume thresholding, and statistical outlier detection. First, by assuming bilateral symmetry in the skeletal system, differences in volume exceeding 50% indicate segmentation issues for symmetrical bones like ribs, clavicles, pelvis, and femurs. Up to two discrepancies among the 16 sets of symmetrical bones evaluated, which include 12 pairs of ribs and other paired skeletal structures were allowed. The bones of the arms were excluded due to position variations. Second, the organ volume is computed after segmentation to exclude patients with unusual positioning or incomplete scans given more than 25% of segmented structures with zero volume. Third, in the statistical outlier detection method, Hartigan's dip test was applied to selected organs to determine if the volume distribution is multimodal. Outliers were identified in unimodal distributions by the interquartile range and in multimodal distributions by Gaussian mixture models. Organs with >90% outlier probabilities were flagged.

In our final quality control process, 2D renderings of the segmentation volumes were examined by a physician for any disparities. Any observed anomalies were flagged. This methodology exemplifies a 'human-in-the-loop' approach, combining expert oversight with technical optimizations for expedited yet thorough analysis.

2.4 3D Representation & Phantoms Smoothing

The Quality Control module employs stringent acceptance criteria to ensure high fidelity in segmentation results. Cases are rejected if they exhibit major faults, such as failures in bilateral symmetry, partial or incomplete scans as evidenced by volume checks, and failure in segmenting at least two organs identified by statistical clustering method. Only cases that meet these criteria

proceed to the 3D representation module, which transforms the voxelized segmentation masks into smooth polygon meshes. Cases with minor irregularities, such as fewer segmented organs, are documented in the metadata along with a quality rating from a medical doctor, ensuring that each model's accuracy and completeness are transparently communicated. GPU-accelerated Laplacian smoothing was used to iteratively refine the vertex positions of 3D meshes while preserving their overall shapes. By utilizing a sparse adjacency matrix to represent mesh connectivity and incorporating a customizable smoothing weight, our approach fine-tunes the degree of smoothing as required. The algorithm, summarized below, converts the input mesh data into tensors, constructs edges, initializes edge weights, and creates a sparse adjacency matrix. Subsequently, row sums are computed for normalization with a main smoothing loop iteratively updating the vertex positions. Finally, the algorithm returns the smoothly refined phantom meshes, effectively achieving our goal of producing faithful representations.

We developed a web application that showcases the developed phantoms interactively. This user-friendly application allows exploration of phantoms filtered by age, sex, and race, with options for

random selection and detailed examination of specific structures as shown in Figure 2.



Figure 2 Web application that shows the 3d anatomical models also allowing user interaction which can be accessed at <https://xcat-2.github.io>.

2.5 Phantom enhancements using mathematical models.

The basic phantoms consist of binary masks of the organs and structures, which can be optionally enhanced with parenchymal texture or refined in accuracy. For example, the lungs may be enhanced with airways and vessels. The public model TotalSegmentator [18] provides the initial seed for airways as the intersection point between each lobe of lungs. A mathematical model [28] is applied to the surfaces segmented from patient CT datasets, and extend the airways and vessels from their initially segmented branches to the terminal branches, incorporating airway wall thickness and optimizing distribution while avoiding intersections between structures.

In another related study, the small intestines were refined by using the gross segmentation of the small intestine to guide the procedural generation of contiguous, tubular surfaces [29] [30]. The initial segmentation was wrapped with a 3D mesh, which constrained the path of a 3D random walk with randomized length and diameter. Finally, the path was smoothed with cubic splines. Such approaches can be used to refine other structures that remain too challenging with current methods.

2.6 Phantoms Integrated to Duke Sim

To generate simulated medical imaging scans, the phantoms produced through our pipeline may be input into DukeSim, our in-house CT simulation platform, or other imaging simulators for different modalities[31]. Leveraging the power of MC-GPU[32], DukeSim simulates a broad range of physics factors including different CT scanner designs and reconstruction algorithms. This simulation process culminates in the generation of highly detailed and realistic simulated CT images.

3. **Results**

3.1 Segmentation

The segmentation model was validated on three public datasets (CT ORG, ABDOMEN 1K, AMOS) and a private dataset (XCAT) using Dice similarity coefficient (DSC) based on the provided organ masks as ground truth. A comparison was made between our model, TotalSegmentator, and the commercial model. The results are shown in box plots (Figure 3), indicating that our model performs similar to the other two models. The commercial model omitted structures that were only partially visible or had low confidence. To avoid skewing the plots, organs with DSC of 0 were

removed. It should be noted that not all models could segment all structures; hence, not all structure DSC values could be reported. Furthermore, qualitative results for phantoms are presented in Figure 4.

3.2 Quality Control

To evaluate the quality of the phantoms, we implemented a multi-step quality control procedure. Initially, we excluded all the patients with age less than 14 years old as the segmentation algorithm was not effective for pediatric patients. The first step leveraged bone symmetry by flagging cases where contralateral bones are more than 50% dissimilar in volume. The method proved effective for preliminary screening: out of 3549 initial cases, 3499 or 99% met the 50% symmetry volume threshold.

The 3499 volumes from the first Quality Control set were passed to the volumetric evaluations of different organs. The goal is to exclude patients in which over 25% of the anatomical structures were missing – that is, organ volumes were zero – due to improper or insufficient scanning. This second step yielded 3406 patient CT scans that were subsequently converted into phantoms.

Among these 3406 patients, the statistical outlier detection approach provided the outlier probability for every organ of every patient. The Figure 5 illustrates the average outlier probabilities for the top 10 organs, separated by gender. Notably, the gallbladder exhibited the highest outlier probability, missing in approximately 16% of cases, predominantly due to cholecystectomies. The other significant outliers identified include the 12th ribs, portal and

splenic veins, smaller structures such as the iliac arteries, and male-specific organs like the prostate and seminal vesicles. These findings align with the visual assessments conducted by the medical doctor.

Approximately 42% of the CT scans were acquired as full body PET/CT scans. These scans with incomplete or missing skull were identified based on outlier probabilities for three structures: brainstem, brain, and skull. Additional filtering was implemented to identify cases where more than two organs per patient exceeded an outlier probability threshold of 0.9, thereby flagging these volumes. Applying all these filters resulted in a curated collection of 3320 patients to provide the most complete, anatomically accurate phantoms. The number of volumes retained after each quality control step is summarized in Table 3. The filtered patients were not discarded, as they may still yield phantoms suitable for many studies. For example, the incomplete skull is irrelevant when creating chest phantoms for pulmonary analysis.

The final step in the process is to select a single volume for patients who have multiple CT volumes available. This is done by identifying the scan with the lowest average outlier probability for each patient who has more than two scans. Following this selection criterion, 2528 unique patients are retained.

Table 3 Volume Retention After Each Quality Control Step

Quality Control Step	Volumes Retained
Total Volumes Reviewed	3581
Age (≥ 14 years)	3549

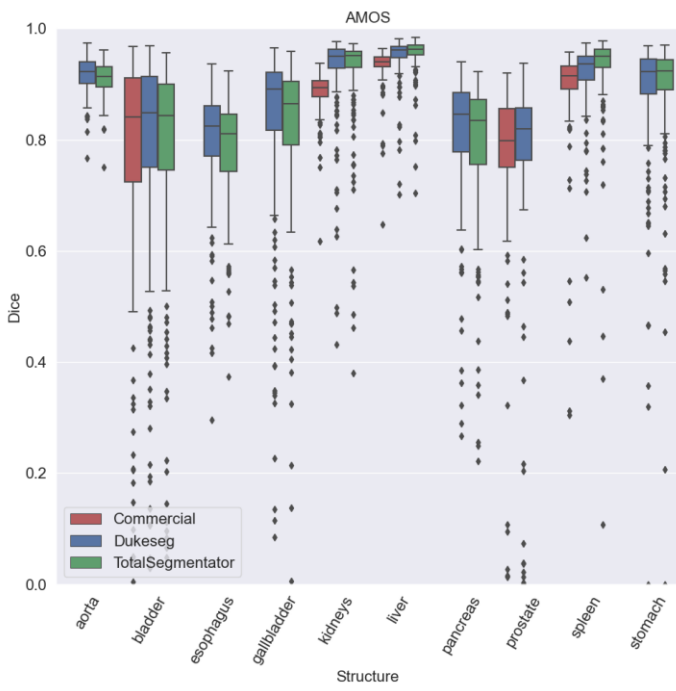
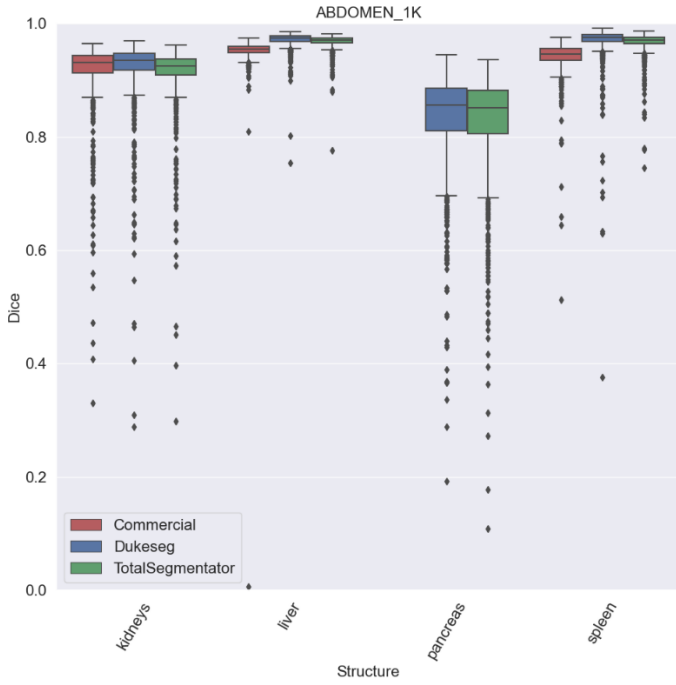
Bilateral Symmetry	3499
Organ Volume	3406
Statistical Clustering	3320

3.3 Patient Demographics and Composition.

In Figure 6 we present the demographic composition of the patient data used to generate the phantoms, reflecting the patient demographics of our institution. The population is primarily White, followed by Black, with a smaller representation of Asian individuals and other races categorized as 'Other'. Additionally, the reliance on PET/CT to provide whole body scans introduces a systematic bias, with a predominance of male subjects, likely attributable to the higher incidence of prostate and lung cancer among males. The average age for the male and female populations in the computational models are 64.9 (14.0) and 61.2 (15.6) years, respectively. Furthermore, the heatmap shown in Figure 7 represents the frequency of height and weight within the virtual patient population. Approximately $\frac{3}{4}$ of the patients were concentrated around weight between 70 and 100 kg and height between 1.7 and 1.9 meters. The physical traits that are most common among the patient cohort that contribute to the phantom dataset are shown in this visualization.

In Figure 8, we present the mean organ volume and standard deviation for selected organs across our phantom population. Notably, structures such as the gallbladder exhibit a significantly higher standard deviation, reflecting the variability of that small organ and the fact that some patients had undergone gallbladder removal surgery.

In Figure 9, we present a range of phantoms that exhibit a wide variety of age, race, BMI, and sex characteristics to emphasize the diversity within our phantom collection. Muscles and fat have been omitted from these visualizations to maintain an unobstructed view of the internal anatomical features. In the current iteration, bones located below the femur and other smaller bones have not been segmented.



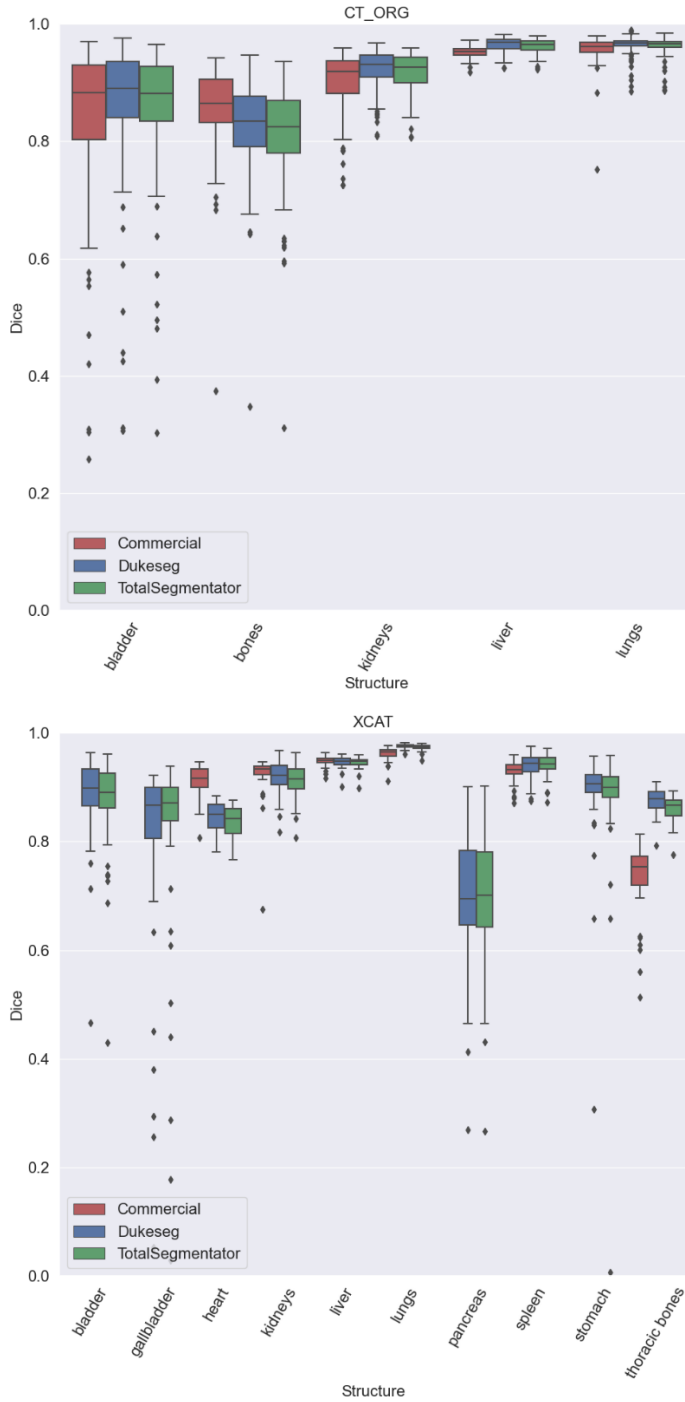


Figure 3 Boxplots that shows the performance of DukeSeg with other public and private model. Performance is compared on three public datasets ABDOMEN_1K, AMOS, CT_ORG and a private dataset XCAT. Certain structures like ribs, scapula, sternum were combined as thoracic bones for XCAT dataset and minor structures such as duodenum and adrenal glands were omitted for AMOS dataset for clarity.

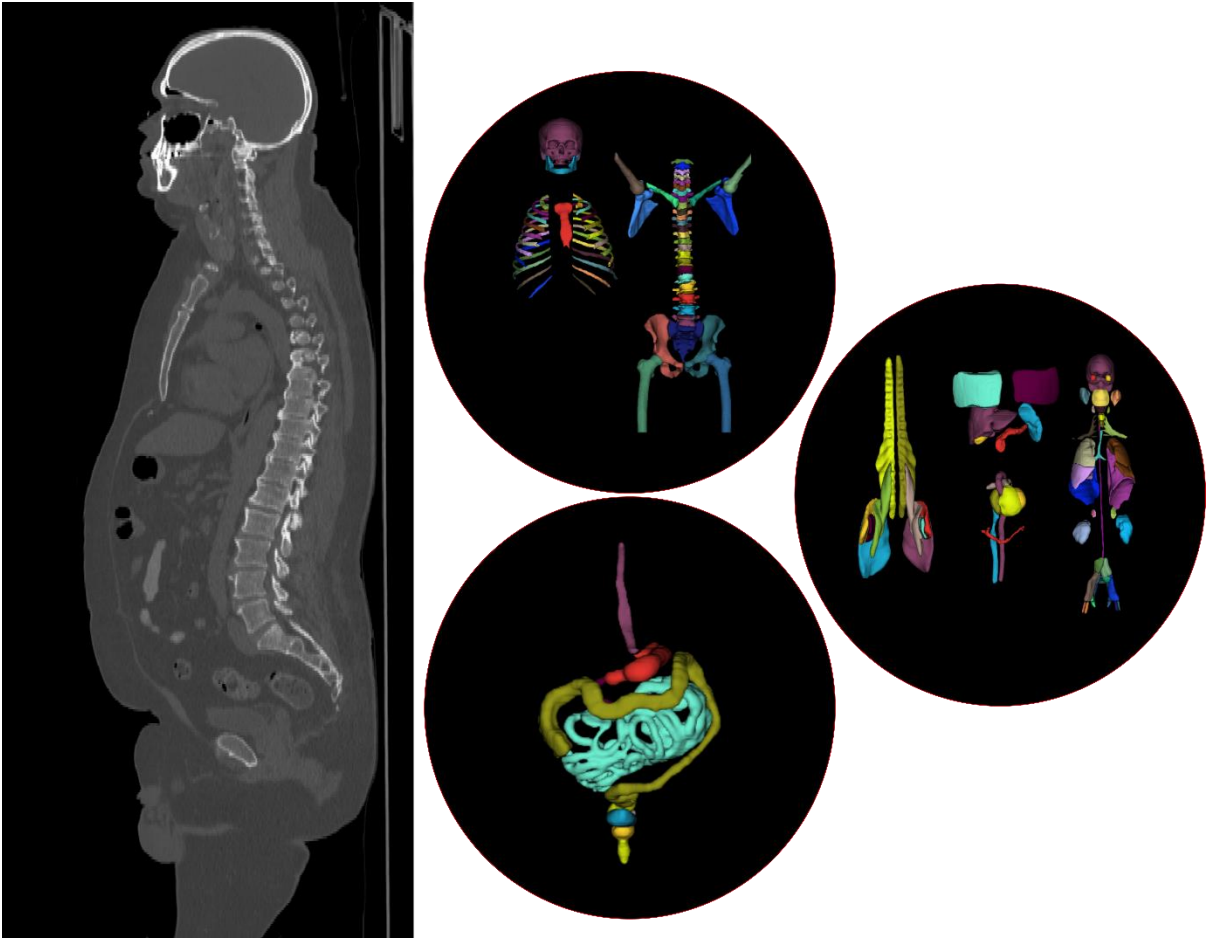


Figure 4 Qualitative comparison of segmentation results: the CT image is displayed on the left, with the outputs of the three segmentation models (Skeleton, Abdomen and Others) from Dukeseqv1 illustrated in three circles on the right, showcasing their performance in delineating the targeted anatomical structures.

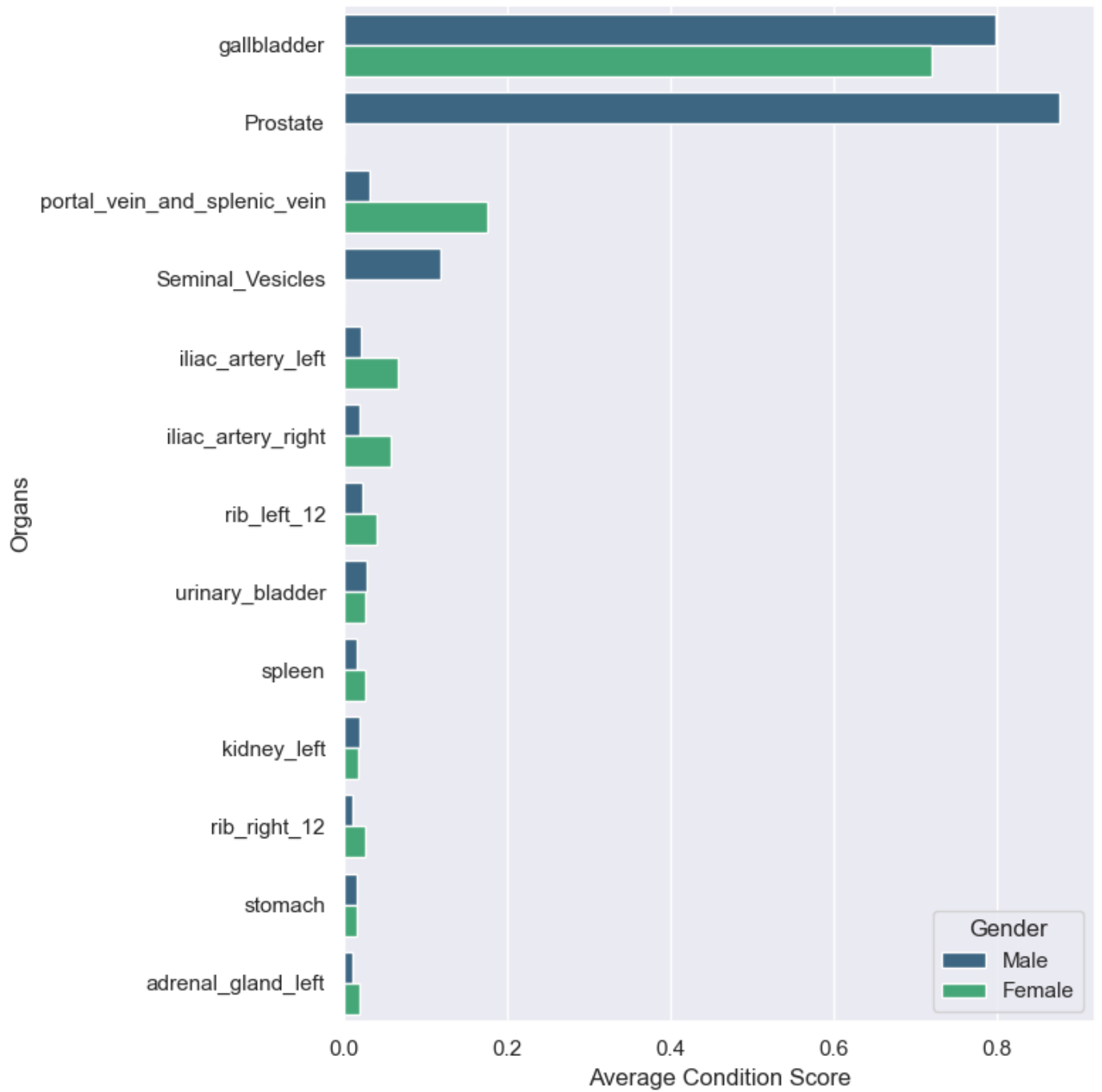


Figure 5 Top outlier organs identified by Statistical Clustering approach for both gender.

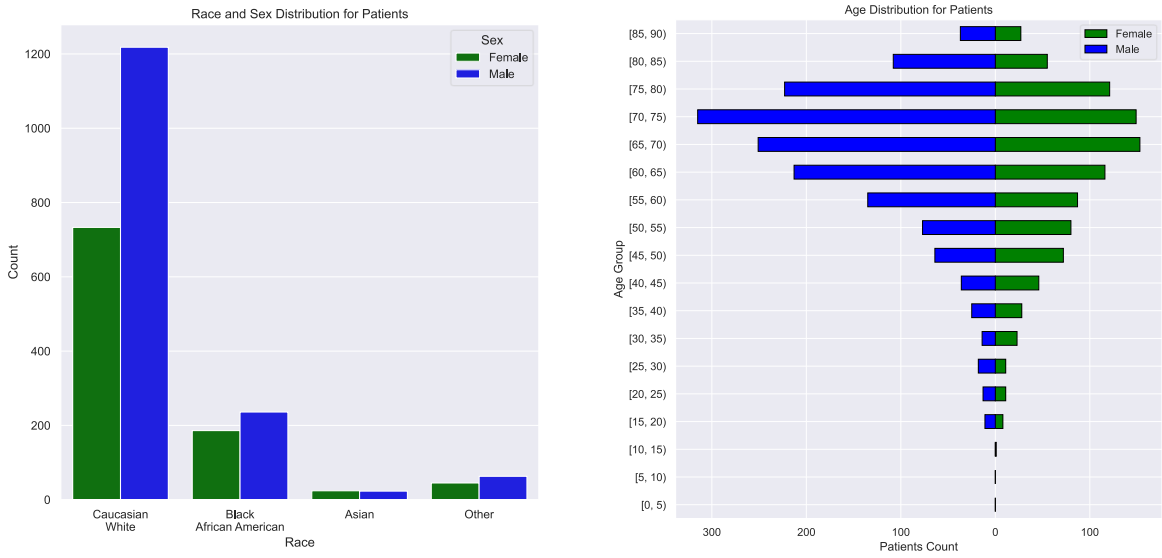


Figure 6 Race and Age distribution for patients which are used to create digital twins.

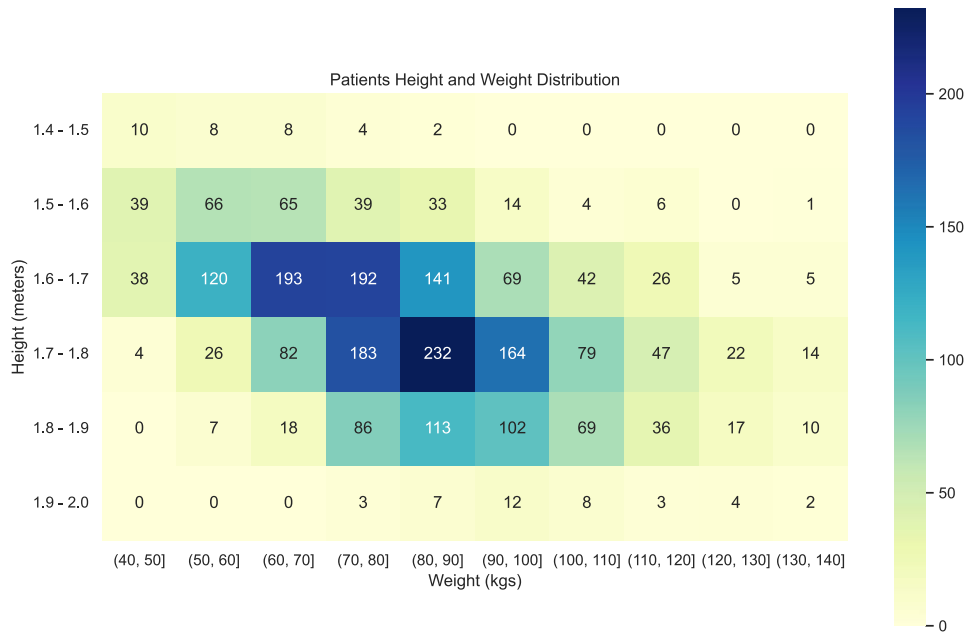


Figure 7 Persons Height and Weight Distribution that pass all Quality Control

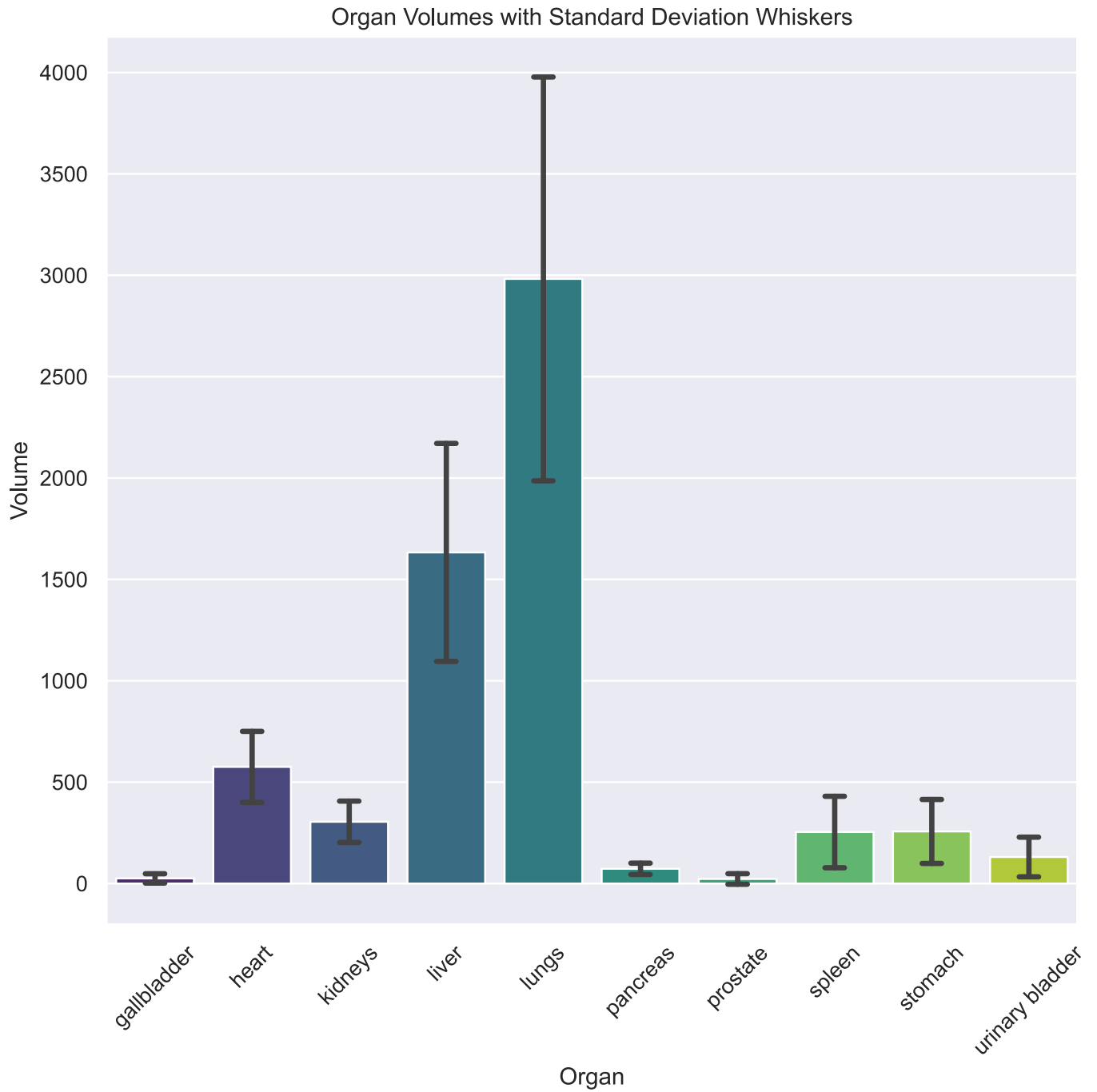
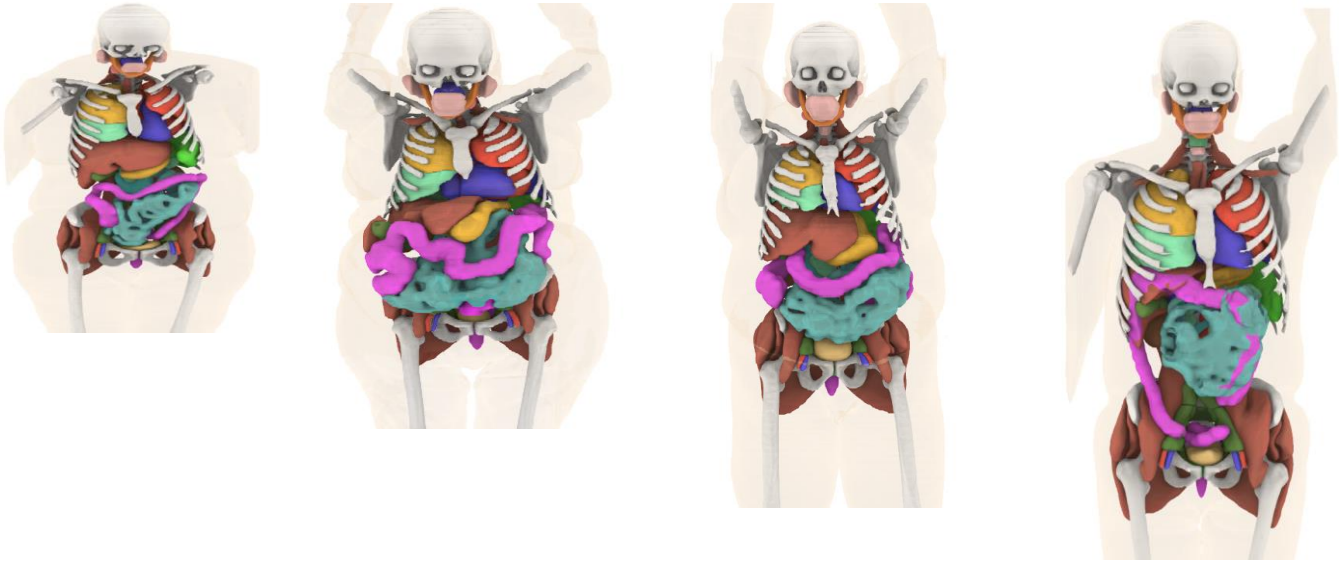


Figure 8 Organ Volume for major organs with range of mean and standard deviation.



XCAT2_00277
 Sex : Female
 Age : 69
 Height : 1.16 meters
 Weight : 75 kg
 Race: White

XCAT2_02380
 Sex : Female
 Age : 82
 Height : 1.47 meters
 Weight : 73 kg
 Race : White

XCAT2_00074
 Sex : Male
 Age : 68
 Height : 1.75 meters
 Weight : 113 kg
 Race : Black

XCAT2_00294
 Sex : Male
 Age : 44
 Height : 1.93 meters
 Weight : 88 kg
 Race : White

Figure 9 3D renderings of 4 computational phantoms in increasing order by height.

4. Discussion

In this study, we devised a framework for generating highly detailed patient-specific anatomical models, which represent a form of human digital twins appropriate for research in medical imaging. A significant challenge in scaling the phantom generation process was the manual segmentation of patient CT scans, which was prohibitively time-consuming and labor intensive. To overcome this bottleneck, we developed a deep learning model capable of segmenting up to 140 structures from patient CT volumes, which significantly enhanced the scalability of the phantom generation process. Furthermore, we implemented an automated quality control module to exclude or flag likely instances of segmentation failure, allowing the new phantoms to be based on the highest quality subset while still preserving the larger population for applications suitable to the end user. This demonstration of scalability in phantom creation is crucial for use in virtual imaging trials, which necessitate a large and diverse sample size to ensure generalizability.

Building a fully automated segmentation pipeline poses significant challenges due to the inherent lack of high-quality image data with validated labels. Even widely used public CT datasets contain incorrect labels, which reduces the model training effectiveness as well as the subsequent application performance. This study showed that quality control during the segmentation of 140 structures presents a formidable task due to the variations in size, shape, and appearance of these structures. Consequently, a single quality control algorithm was proved insufficient. For instance, a quality control measure for small structures like ribs may not be suitable for larger structures like the liver. The development of a multi-step quality control process improved the results for this study and may also benefit other segmentation studies.

We have employed a multi-model approach for segmenting the 140 structures, which offers two significant advantages. Firstly, instead of retraining the entire model, we can selectively train only the model of interest. For instance, the skeletal system segmentation model achieved superior results, so we locked down this model early. However, there was still room for improvement in segmenting structures such as the large intestine and small intestine. Since these abdominal structures were segmented using the same model, we were able to focus on enhancing that specific model in further iterations. The second advantage of this design choice pertains to computational efficiency. Our studies involve full body CT scans, typically sized at 512x512x2000. Storing probabilities for 140 classes for each voxel becomes inconvenient in terms of scalability. Therefore, by employing multiple models, we mitigate the storage challenges associated with inferring and storing probabilities for the entire volume, thereby improving computational efficiency.

The web application developed to display diverse sets of anatomical model allows not only scientific inquiry but also may be helpful as an educational resource, introducing trainees and enthusiasts to detailed human

anatomy through a dynamic and engaging platform. This initiative marks a significant stride in enhancing accessibility and interactivity in anatomical education.

5. **Limitations and Future Work**

Our phantoms are derived from CT images, which are obtained from patients undergoing medical evaluations rather than from the general healthy population. This selection bias presents a challenge in representing typical organ volumes accurately. Moreover, the reliance on PET/CT scans to provide whole body coverage led to more male patients. For many applications, the large size of the phantom cohort allows sub-sampling to mitigate these biases. The dataset included surgical removals such as for the gallbladder or kidney, which can be restored such as using diffusion models. Note however that our current patient-specific phantoms faithfully represent the actual patient anatomy.

Although the segmentation model was trained and validated on multiple datasets, the final phantoms were created only using data from Duke University Health System because of the challenges to acquire large clinical datasets with demographic/clinical data that include CT images, guide the quality control with radiologist report. This restricted the generated phantoms to predominantly represent the demographic distribution of one academic institution in the Southeastern US, which may not reflect broader demographics. To address this issue and enhance the model's generalizability, future efforts are put to validate our segmentation model using a more diverse dataset from multiple medical centers. Future studies will expand the scope to improve segmentation techniques and integrate more structures into the computational model by refining the segmentation algorithm or incorporating generative methods to fill in anatomical gaps.

6. **Conclusion**

We build computational phantoms using the fusion of deep learning techniques and stringent quality control and announce their public release. We have designed an interactive web application with the power to filter and display phantoms by age, sex, and race. These phantoms will facilitate the conducting of virtual imaging trials for a wide range of clinical applications. This versatility underscores the potential of our phantoms to revolutionize virtual trials and beyond, offering a wide range of possibilities for research and development in the field of medical imaging.

Data availability

The anthropomorphic phantoms are publicly available via licensing at <https://cvit.duke.edu/resources/>.

Code availability

The code for generating phantoms, which encompasses segmentation, quality control (QC), and meshing, is available at <https://xcat-2.github.io>. Modules for enhancing phantoms, including the addition of lesions and tissue textures, as well as CT simulation packages, are accessible upon request for research purposes.

Acknowledgments

This work was funded by the Center for Virtual Imaging Trials, NIH/NIBIB P41EB028744, and NIH/NCI R01CA261457.

References

1. Barufaldi, B., et al., *Virtual clinical trials in medical imaging system evaluation and optimisation*. Radiation Protection Dosimetry, 2021. **195**(3-4): p. 363-371.
2. Tushar, F.I., et al., *Data diversity and virtual imaging in AI-based diagnosis: A case study based on COVID-19*. arXiv preprint arXiv:2308.09730, 2023.
3. Tushar, F.I., et al. *Virtual NLST: towards replicating national lung screening trial*. in *Medical Imaging 2024: Physics of Medical Imaging*. 2024. SPIE.
4. Abadi, E., et al., *Virtual clinical trials in medical imaging: a review*. Journal of Medical Imaging, 2020. **7**(4): p. 042805-042805.
5. Fisher Jr, H., *Variation of dose delivered by ¹³⁷Cs as a function of body size from infancy to adulthood*. ORNL-4007, 1966: p. 221-228.
6. Segars, W.P., et al., *4D XCAT phantom for multimodality imaging research*. Medical physics, 2010. **37**(9): p. 4902-4915.
7. Ackerman, M.J., *The visible human project*. Proceedings of the IEEE, 1998. **86**(3): p. 504-511.
8. Xu, X., T.-C. Chao, and A. Bozkurt, *VIP-Man: an image-based whole-body adult male model constructed from color photographs of the Visible Human Project for multi-particle Monte Carlo calculations*. Health physics, 2000. **78**(5): p. 476-486.
9. Lee, C., et al., *Hybrid computational phantoms of the male and female newborn patient: NURBS-based whole-body models*. Physics in Medicine & Biology, 2007. **52**(12): p. 3309.
10. Segars, W., et al., *Population of anatomically variable 4D XCAT adult phantoms for imaging research and optimization*. Medical physics, 2013. **40**(4): p. 043701.
11. Segars, W., et al., *The development of a population of 4D pediatric XCAT phantoms for imaging research and optimization*. Medical physics, 2015. **42**(8): p. 4719-4726.
12. Bolch, W., *Computational models of human anatomy*, in *Monte Carlo Calculations in Nuclear Medicine (Second Edition) Therapeutic applications*. 2022, IOP Publishing Bristol, UK. p. 5-1-5-43.
13. Akhavanallaf, A., et al., *An update on computational anthropomorphic anatomical models*. Digital Health, 2022. **8**: p. 20552076221111941.
14. Young, S., et al., *A virtual trial framework for quantifying the detectability of masses in breast tomosynthesis projection data*. Medical physics, 2013. **40**(5): p. 051914.
15. Fukunaga, K. and R.R. Hayes, *Effects of sample size in classifier design*. IEEE Transactions on Pattern Analysis and Machine Intelligence, 1989. **11**(8): p. 873-885.
16. Park, S., G. Zhang, and K.J. Myers, *Comparison of channel methods and observer models for the task-based assessment of multi-projection imaging in the presence of structured anatomical noise*. IEEE transactions on medical imaging, 2016. **35**(6): p. 1431-1442.
17. Fu, W., et al., *iPhantom: a framework for automated creation of individualized computational phantoms and its application to CT organ dosimetry*. IEEE journal of biomedical and health informatics, 2021. **25**(8): p. 3061-3072.
18. Wasserthal, J., et al., *Totalsegmentator: Robust segmentation of 104 anatomic structures in ct images*. Radiology: Artificial Intelligence, 2023. **5**(5).

19. Liu, J., et al. *Clip-driven universal model for organ segmentation and tumor detection*. in *Proceedings of the IEEE/CVF International Conference on Computer Vision*. 2023.
20. Kirillov, A., et al. *Segment anything*. in *Proceedings of the IEEE/CVF International Conference on Computer Vision*. 2023.
21. Ma, J., et al., *Segment anything in medical images*. *Nature Communications*, 2024. **15**(1): p. 654.
22. Sundar, L.K.S., et al., *Fully automated, semantic segmentation of whole-body 18F-FDG PET/CT images based on data-centric artificial intelligence*. *Journal of Nuclear Medicine*, 2022. **63**(12): p. 1941-1948.
23. Mazurowski, M.A., et al., *Segment anything model for medical image analysis: an experimental study*. *Medical Image Analysis*, 2023. **89**: p. 102918.
24. Rister, B., et al., *CT-ORG, a new dataset for multiple organ segmentation in computed tomography*. *Scientific Data*, 2020. **7**(1): p. 381.
25. Ma, J., et al., *Abdomenct-1k: Is abdominal organ segmentation a solved problem?* *IEEE Transactions on Pattern Analysis and Machine Intelligence*, 2021. **44**(10): p. 6695-6714.
26. Ji, Y., et al., *Amos: A large-scale abdominal multi-organ benchmark for versatile medical image segmentation*. *Advances in Neural Information Processing Systems*, 2022. **35**: p. 36722-36732.
27. Isensee, F., et al., *nnU-Net: a self-configuring method for deep learning-based biomedical image segmentation*. *Nature methods*, 2021. **18**(2): p. 203-211.
28. Abadi, E., et al., *Modeling lung architecture in the XCAT series of phantoms: physiologically based airways, arteries and veins*. *IEEE transactions on medical imaging*, 2017. **37**(3): p. 693-702.
29. Yeom, Y.S., et al., *New small-intestine modeling method for surface-based computational human phantoms*. *Journal of Radiological Protection*, 2016. **36**(2): p. 230.
30. Kim, D., et al. *Random walk small intestine models for virtual patient populations*. in *Medical Imaging 2024: Physics of Medical Imaging*. 2024. SPIE.
31. Abadi, E., et al., *DukeSim: a realistic, rapid, and scanner-specific simulation framework in computed tomography*. *IEEE transactions on medical imaging*, 2018. **38**(6): p. 1457-1465.
32. Badal, A. and A. Badano, *Accelerating Monte Carlo simulations of photon transport in a voxelized geometry using a massively parallel graphics processing unit*. *Medical physics*, 2009. **36**(11): p. 4878-4880.